

# A useful canonical form for low dimensional attractors

Nicola Romanazzi<sup>1</sup>, Valerie Messenger<sup>2</sup>, Christophe Letellier<sup>2</sup>, Marc Lefranc<sup>3</sup>, and Robert Gilmore<sup>1</sup>

<sup>1</sup>*Physics Department, Drexel University, Philadelphia, Pennsylvania 19104, USA,*

<sup>2</sup>*CORIA UMR 6614 - Université de Rouen, BP 12,*

*Av. de l'Université, Saint-Etienne du Rouvray cedex, France, and*

<sup>3</sup>*PHLAM-CNRS, Université de Sciences et Technologies de Lille*

(Dated: August 3, 2007, *Physical Review E*: To be submitted.)

Powerful computational techniques have been developed to study chaotic attractors that are generated by stretching and folding processes. These include relative rotation rates for determining the organization of unstable periodic orbits and simplex distortion procedures for estimating the topological entropy of these orbits. These methods are useful for attractors contained in a genus-one torus  $D^2 \times S^1$ , where all unstable orbits have a braid representation. We extend these methods to attractors in higher-genus tori (e.g., the Lorenz attractor) by mapping higher-genus attractors to diffeomorphic attractors that have a braid representation. We illustrate by computing the topological measures for orbits in the Lorenz attractor.

## I. INTRODUCTION

It has been known for many years that the unstable periodic orbits that exist in abundance in a strange attractor serve as a skeleton for the attractor [1]. Once the organization of these orbits is known, the topological structure of the attractor is known. The topological organization is determined by the Gauss linking number in three dimensions, where this integer is rigidly and uniquely determined by two orbits that have no common points. An even more refined topological invariant is the spectrum of relative rotation rates for either a single orbit or a pair of orbits. This invariant (RRR here and below) carries more information than the linking number [2–6].

The linking number is a topological invariant in  $R^3$  while the RRR exist naturally in phase spaces with a different global topological structure. This is the torus  $R^2 \times S^1$  or  $D^2 \times S^1$ , where  $D^2 \subset R^2$  is a disk of finite diameter in the plane. In order to compute linking numbers from RRR it is necessary first to map  $D^2 \times S^1 \rightarrow R^3$ . This is usually done without explicitly acknowledging the embedding used, which is always the natural embedding [7]. Once such an embedding has been made it is possible to compute the linking number of a pair of orbits from their RRR. The relation is  $L(A, B) = \sum_{i,j}^{p_A, p_B} RRR_{i,j}(A, B)$  [2, 5, 6]. Here  $A$  and  $B$  are orbits of periods  $p_A$  and  $p_B$ ,  $1 \leq i \leq p_A$ ,  $1 \leq j \leq p_B$ , and  $RRR_{i,j}(A, B)$  is the relative rotation rate of the pair  $(A, B)$  where  $i$  and  $j$  index the  $i$ th and  $j$ th intersections of  $A$  and  $B$  with some Poincaré section.

The RRR are very powerful for describing chaotic attractors that exist in a bounding torus of genus one [8, 9]. Such attractors are generated by stretching and folding mechanisms - tearing does not take place. Such attractors include the Rössler attractor and many periodically driven two-dimensional nonlinear oscillators such as the

Duffing and van der Pol systems, as well as autonomous systems generating chaotic attractors with one “hole in the middle.” Attractors generated by stretching and tearing mechanisms (e.g., Lorenz, Shimizu-Morioka [10–12]) are generally not contained in genus-one bounding tori [13, 14], so that relative rotation rates are not available for a refined description of their orbits.

New computational methods (deformed simplices) have recently been introduced that greatly simplify the computation of the topological entropy of periodic orbits in chaotic attractors [15]. The computations are simplified because the very nonintuitive traintrack algorithm [26–28] is replaced by a much more intuitive approach that shows how an orbit deforms the surrounding phase (the simplices in the phase space) under iteration. These algorithms have been applied only to flows generated by stretching and folding mechanisms. They appear not to be directly applicable to flows such as those that exist in bounding tori of genus  $g > 1$ .

In this work we show that it is possible to map a flow contained in a genus  $g (> 1)$  torus into a diffeomorphic flow contained in a genus-one bounding torus. This makes it possible to extend the computational tools developed for the class of flows generated by stretching and folding mechanisms to the class of flows generated by stretching and squeezing (i.e., tearing) mechanisms. As a result, more refined descriptions of orbit organization using RRR rather than LN are possible. It also becomes possible to extend the simplex method for computing topological entropy to more complex dynamical systems.

In Sect. II we briefly review how RRR are computed and we describe how simplex deformation is used to estimate topological entropy. In Sect. III we describe how to construct a braid representation for a genus- $g$  torus, and we do so explicitly for a Lorenz branched manifold.

In Sect. IV we show how to use a multicomponent return map on  $g-1$  branch lines to determine properties of periodic orbits in a genus- $g$  attractor. This information, together with the braid representation of the Lorenz template, is used to construct the RRR (in Sect. IV) and the topological entropy (in Sect. V) for all orbits to period six in the Lorenz attractor. Our results are summarized in Sect. VII.

## II. REVIEW OF TOPOLOGICAL INVARIANTS

In this section we describe three topological invariants that can be constructed for orbits in a strange attractor that is generated by a stretching and folding mechanism. Such attractors exist within a genus-one torus  $D^2 \times S^1$ . In such cases a Poincaré surface of section can be chosen transverse to the flow at phase angle  $\phi \in S^1$ ,  $0 \leq \phi \leq 2\pi$  [8, 9]. Two periodic orbits  $A$  and  $B$  intersect any Poincaré section at points  $i = 1, 2, \dots, p_A$  and  $j = 1, 2, \dots, p_B$ . When a difference vector  $\mathbf{v}_{ij}$  between intersection  $i$  of orbit  $A$  and  $j$  of orbit  $B$  is propagated forward for  $p_A \times p_B$  periods, it returns to its initial condition by rotating through an integer number  $n_{ij}$  of turns in the Poincaré section (as  $\phi$  goes from 0 to  $2\pi(p_A \times p_B)$ ) [2, 5, 6]. The ratio  $n_{ij}/(p_A \times p_B) = RRR_{ij}(A, B)$  is the relative rotation rate of the two orbits, starting from initial conditions  $i$  on  $A$  and  $j$  on  $B$ . The RRR from different initial conditions need not be the same; these rational fractions can have no more than  $\text{gcd}(p_A, p_B)$  different values, where  $\text{gcd}$  is the greatest common divisor of its two integer arguments. The relative rotation rates of an orbit with itself (SRRR) are defined in the same way. The self relative rotation rate  $RRR_{ii}(A, A)$  is defined as the local torsion of the branch containing the orbit segment starting at  $i$ .

The linking number of orbits  $A$  and  $B$  in  $D^2 \times S^1$  is not defined, as this invariant exists in  $R^3$ . When the torus  $D^2 \times S^1$  is mapped into  $R^3$ , this mapping also carries the orbits  $A$  and  $B$  into  $R^3$ , so that their linking number can be computed in the embedding. When the mapping is the natural embedding, the linking number of the two orbits  $A$  and  $B$  in  $R^3$  is equal to the sum of the RRR of the two orbits in  $D^2 \times S^1$  [16]:

$$L(A, B) \text{ in } R^3 = \sum_{i,j}^{p_A, p_B} RRR_{i,j}(A, B) \text{ in } D^2 \times S^1 \quad (1)$$

Another topological invariant for single or multiple orbits in  $D^2 \times S^1$  is topological entropy  $h_T$ . This single real number estimates the exponential growth in the numbers of orbits present of period  $p$  caused by one or a predetermined set of orbits [1]. The intersections of the single (or several) orbits with a Poincaré section are identified and the deformation of these intersections as the phase  $\phi$  increases from 0 to  $2\pi$  is determined. These intersections are used to make a simplicial decomposition of the disk

$D^2$ . As intersections of vertices with edges occur, modifications in the decomposition are carried out in search for an asymptotic set of basic edges. The basic edges are mapped into each other, or unions of each other, under a forward iteration. A transition matrix is constructed, and the logarithm of the largest eigenvalue  $\lambda_{Max}$  of this matrix provides a (lower) limit on the topological entropy for the initial orbit or union of orbits;  $h_T \geq \log(\lambda_{Max})$  [15].

These two topological invariants — a set of  $p_A \times p_B$  rational fractions  $RRR_{i,j}(A, B)$  and a real number  $h_T$  are computed by projecting the flow in  $D^2 \times S^1$  in two different ways. Define coordinates  $(x, y)$  on the disk  $D^2$ . To construct the RRR it is useful to project the orbits along the  $y$  direction into the  $(x, \phi)$  plane, indicating over- and under-crossings in the usual way. Then the RRR are computed by counting crossings and dividing by twice the number of forward iterations. To construct  $h_T$  it is useful to project into the  $(x, y)$  plane and follow the motion of the orbit intersections with a Poincaré section as the Poincaré section moves along the axis of the torus. In this sense these two topological indices are dual to each other.

## III. BRAID REPRESENTATION OF BRANCHED MANIFOLDS

Any single closed orbit (or knot) can be smoothly deformed to a very special canonical form called a braid form (Alexander's theorem [17]). This is distinguished by having all crossings on one side, by convention near the observer. The return flow, on the other side, simply exists to ensure periodic boundary conditions. In its braid form the knot can be represented algebraically and it is a simple matter to count crossings [17, 18].

It is not generally true that two or more knots can simultaneously be deformed to braid canonical form. Nor is it true that a branched manifold can be smoothly deformed to braid canonical form [19]. What is true is that a branched manifold contained within a genus-one bounding torus has a canonical braid form. It is also true that if all the unstable periodic orbits in a strange attractor, or on the branched manifold that represents this strange attractor, can simultaneously be smoothly deformed to braid form, then the strange attractor and its branched manifold are bounded by the surface of a genus-one torus [16].

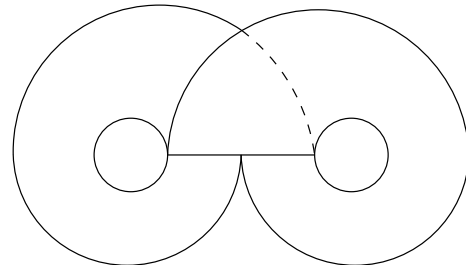
As a particular example, the branched manifold for the Lorenz dynamical system at standard control parameter values cannot be smoothly deformed to a braid canonical form [19–21]. As a result, the topological methods reviewed in Sect. II cannot be applied directly to this dynamical system. These methods can be used if it is possible to construct a diffeomorphism that relates the Lorenz flow (or branched manifold) to a flow, or branched manifold, that can be embedded in a genus-one bounding torus.

This can be done in general, but not smoothly. The construction involves discontinuous operations, such as cutting and pasting. We illustrate how for the Lorenz branched manifold. Fig. 1(a) shows a branched manifold that describes the Lorenz flow ([6], Fig. 8.3, p. 329 and Fig. 8.4, p. 330; [22], Fig. ?; [12], Fig. ??). The symmetry axis is in the plane of this projection. A different planar projection is obtained by rotating the “ear” on the right by  $\pi$  radians out of the plane of the figure. This projection is shown in Fig. 1(b) ([6], Fig. 8.3, p. 329 and Fig. 8.4, p. 330; [22], Fig. ?; [12], Fig. ??). The symmetry axis is perpendicular to the plane of this projection. In Fig. 1(c) we show the boundary of a genus-three torus that contains the branched manifolds shown in (a) and (b) ([9], Fig. ?). The two circles shown on the boundary are meridians that can be chosen so that the flow within the torus is everywhere transverse. These meridians bound disjoint two-dimensional surfaces whose union constitutes the global Poincaré surface of section for this dynamical system.

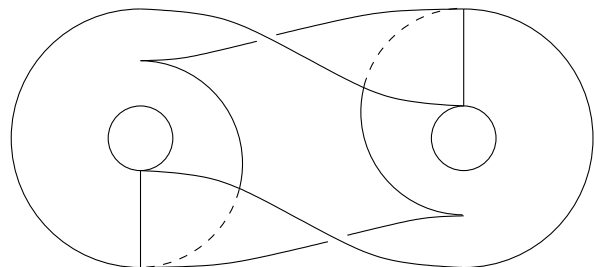
The representation of the flow presented in Fig. 1 can be transformed to braid form in a systematic way. We begin by recalling that any branched manifold can be constructed from splitting and joining units (Fig. III, top row). These units are combined outputs to inputs, with no free ends [5, 6, 20, 21]. In the same way, bounding tori [8, 9] are constructed from splitting and joining  $Y$  junctions (Fig. III, bottom row) [23]. The rules for construction of genus- $g$  tori from these basic units are even simpler. They are most simply visualized as follows. Color the single input port in a splitting junction red and the single output port for a joining unit green. Color the pair of output ports in a splitting junction blue and the pair of input ports in a joining junction orange. Red and green are complementary colors, as are blue and orange. The genus-3 bounding torus shown in Fig. 3 is constructed by taking two splitting junctions and two joining junctions and joining complementary colors. The two components of the Poincaré surface of section exist at the red-green junctions.

To construct a braid representation of this bounding torus (and any branched manifold contained within it) proceed as follows. Cut the bounding torus at the red-green junctions and deform it so that the red circles are placed in a plane at  $s = 0$  and its matching green circle is placed directly below it in a plane at  $s = 1$ . This representation is shown for the genus-3 bounding torus in Fig. 4. In this way the components of the Poincaré surface of section are matched at  $s = 0$  and  $s = 1$ . This constitutes the “front” of the braid representation of this flow. A return flow to each component completes the transformation of the bounding torus (and any branched manifold in it) to a braid representation. The return flow, from  $s = 1$  back to  $s = 0$ , simply preserves boundary conditions in exactly the same way as in a braid representation for knots [12, 17, 18, 24].

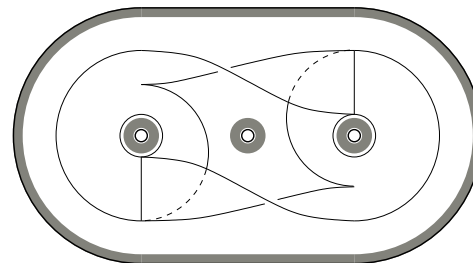
The transformation of a genus- $g$  bounding torus from its canonical representation [8, 9] to its braid represen-



(a) Branched for the Lorenz attractor



(b) Another representation of this branched manifold



(c) Genus-3 bounding torus with branched manifold inside

FIG. 1: (a) Cardboard model for the Lorenz flow is also a branched manifold describing the flow. This has rotation symmetry around the  $Z$  axis. (b) Another representation of the Lorenz branched manifold obtained by rotating the “right ear” by  $\pi$  radians. This representation has rotation symmetry about an axis perpendicular to the projection plane. (c) A genus-3 bounding torus that contains the Lorenz branched manifold. The two circles (meridians) bound the two components of the global Poincaré surface of section.

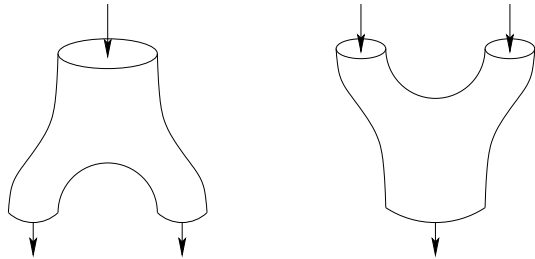


FIG. 2: (Top) Branched manifolds are constructed from splitting and joining units. (Bottom) Bounding tori of genus  $g > 1$  can be composed of  $Y$  junctions of the form shown. Splitting units have one input port (red) and two output ports (blue) while joining units have two input ports (orange) and a single output port (green).

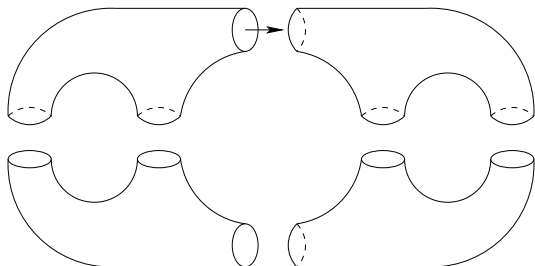


FIG. 3: The genus-3 torus containing the flow that generates the Lorenz attractor can be decomposed into two splitting junctions and two joining junctions.

tation follows exactly the steps described above for the genus-3 bounding torus.

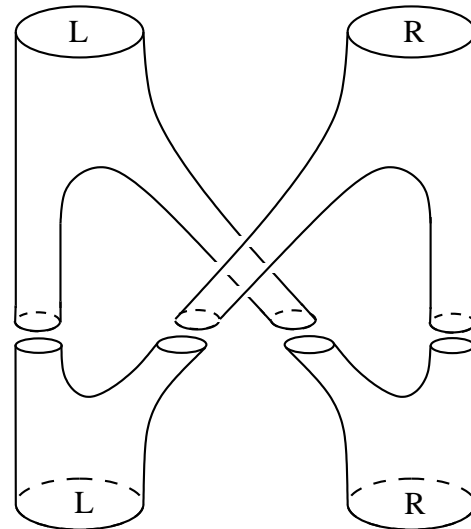


FIG. 4: Disk  $L$  of the global Poincaré surface of section is the source for flows to two different parts of the phase space. This is represented by the “splitting” junction (inverted  $Y$ , [23]). Similarly for  $R$ . Flows from different parts of the phase space approach disk  $L$  through the “joining” junction ( $Y$ , [23]). Similarly for  $R$ . The return flow from  $L$  to  $L$  and from  $R$  to  $R$  occurs in a genus-one bounding torus, and must satisfy periodic boundary conditions.

The branched manifold describing Lorenz dynamics is presented in braid form as shown in Fig. 5. In this figure a disk is shown on the left at  $s = 0$ . The disk has radius greater than  $a + b + 1$  and is large enough to contain the return flow in the two separate tubes joining  $L$  to  $L$  and  $R$  to  $R$ . The disks  $L$  and  $R$  each have diameter 1. The two branch lines, one in each disk  $L$  and  $R$ , are shown. The branch line labeled  $L$  occupies the interval  $a + b$  and  $a + b + 1$ ,  $y = 0$  and that labeled  $R$  occupies the interval  $-(a + b)$  and  $-(a + b + 1)$ ,  $y = 0$ . The first return map of these two intervals is shown in Fig. 6. Points on the branch lines are identified by a single coordinate. For example, the coordinate  $R(x)$  describes a point on the branch line  $R$  a distance  $0 \leq x \leq 1$  from the inner edge of the branched manifold. It’s coordinate in Fig. 4 is  $(-(a + b + x), 0)$ .

According to the return map of Fig. 6, points on either branch line with coordinate  $0 \leq x < \frac{1}{2}$  return to the same branch line; those with coordinate  $\frac{1}{2} < x \leq 1$  flow to the opposite branch line [12–14]. A suspension of the return map of Fig. 6 into a torus is given by the following set of equations:

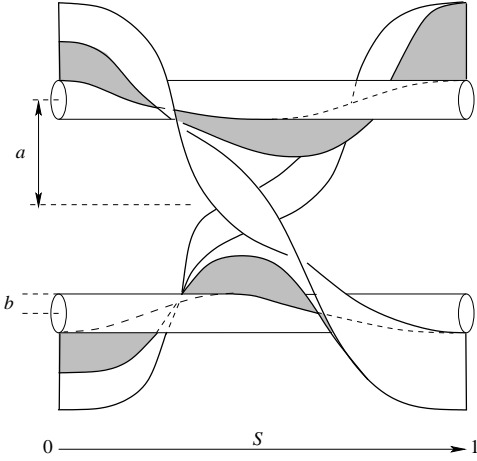


FIG. 5: The large circle of radius  $R > a + b + 1$  on the left contains the two disks  $L$  and  $R$  of the global Poincaré surface of section. Each contains one branch line, also labeled  $L, R$ . The right edge matches the left to satisfy periodic boundary conditions. As the parameter  $s$  increases from  $s = 0$  on the left to  $s = 1$  on the right, the flow moves along the torus. This suspension of the flow in this genus-one torus is diffeomorphic but not isotopic to the flow in the genus-three bounding torus. The flow along the four branches of this branched manifold is defined by Eq. (2). Projection of this branched manifold along the  $s$  direction onto  $(x, y)$  the plane reproduces the structure shown in Fig. 1.

$$\begin{aligned}
 L \quad 0 \leq x < \frac{1}{2} \quad & x(s) = +a + [b + x(1 + s)] \cos 2\pi s \\
 & y(s) = +0 + [b + x(1 + s)] \sin 2\pi s \\
 R \quad 0 \leq x < \frac{1}{2} \quad & x(s) = -a - [b + x(1 + s)] \cos 2\pi s \\
 & y(s) = -0 - [b + x(1 + s)] \sin 2\pi s
 \end{aligned}$$

$$\begin{aligned}
 L \quad \frac{1}{2} < x \leq 1 \quad & x(s) = +[a + b + \frac{3}{4}(1 - \frac{1}{3}s) + \\
 & \quad (x - \frac{3}{4})(1 + s) \cos \pi s] \cos \pi s \\
 & y(s) = +[a + b + \frac{3}{4}(1 - \frac{1}{3}s) + \\
 & \quad (x - \frac{3}{4})(1 + s) \sin \pi s] \sin \pi s \\
 R \quad \frac{1}{2} < x \leq 1 \quad & x(s) = -[a + b + \frac{3}{4}(1 - \frac{1}{3}s) + \\
 & \quad (x - \frac{3}{4})(1 + s) \cos \pi s] \cos \pi s \\
 & y(s) = -[a + b + \frac{3}{4}(1 - \frac{1}{3}s) + \\
 & \quad (x - \frac{3}{4})(1 + s) \sin \pi s] \sin \pi s
 \end{aligned} \tag{2}$$

The trajectory along one of the four branches in this suspension is determined by Eqs. (2) one the branch line ( $L$  or  $R$ ) and the coordinate  $x$  ( $0 \leq x \leq 1$ ) is specified. As  $s$  increases from 0 to 1 the flow extends from the large circle containing the two components of the global Poincaré surface of section on the left to that on the right. From the right, the flow is reinjected to the left, since periodic boundary conditions are enforced (Fig. 5).

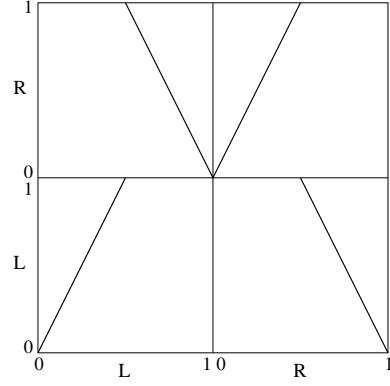


FIG. 6: Return map for the two branch lines in the branched manifold describing Lorenz dynamics [12–14].

TABLE I: Coordinates along the branch lines for orbits to period six in the return map shown in Fig. 6.

Orbit	Coordinates
$L$	$L(0)$
$LR$	$L(\frac{2}{3})R(\frac{2}{3})$
$LLR$	$L(\frac{2}{7})L(\frac{4}{7})R(\frac{6}{7})$
$LLL$	$L(\frac{2}{15})L(\frac{4}{15})L(\frac{8}{15})R(\frac{14}{15})$
$LLRR$	$L(\frac{2}{5})L(\frac{4}{5})R(\frac{2}{5})R(\frac{4}{5})$
$LLLLL$	$L(\frac{2}{31})L(\frac{4}{31})L(\frac{8}{31})L(\frac{16}{31})R(\frac{30}{31})$
$LLLRR$	$L(\frac{6}{31})L(\frac{12}{31})L(\frac{24}{31})R(\frac{14}{31})R(\frac{28}{31})$
$LLRLR$	$L(\frac{10}{31})L(\frac{20}{31})R(\frac{22}{31})L(\frac{18}{31})R(\frac{26}{31})$
$LLLLLL$	$L(\frac{2}{63})L(\frac{4}{63})L(\frac{8}{63})L(\frac{16}{63})L(\frac{32}{63})R(\frac{62}{63})$
$LLLRRR$	$L(\frac{6}{63})L(\frac{12}{63})L(\frac{24}{63})L(\frac{48}{63})R(\frac{30}{63})R(\frac{60}{63})$
$LLLRLR$	$L(\frac{10}{63})L(\frac{20}{63})L(\frac{40}{63})R(\frac{46}{63})L(\frac{34}{63})R(\frac{38}{63})$
$LLLRRR$	$L(\frac{2}{9})L(\frac{4}{9})L(\frac{8}{9})R(\frac{2}{9})R(\frac{4}{9})R(\frac{8}{9})$
$LLRLRR$	$L(\frac{22}{63})L(\frac{44}{63})R(\frac{38}{63})L(\frac{50}{63})R(\frac{26}{63})R(\frac{52}{63})$

#### IV. HOW TO COMPUTE RRR

The first step for computing the RRR of orbits in this braid representation is to locate the orbits in this flow. This can be done by computing the fixed points of the  $p$ th return map for orbits of period  $p$ . To illustrate, the period-five orbit  $LLLRR$  visits the following five points successively on the two branch lines:  $L(\frac{6}{31})L(\frac{12}{31})L(\frac{24}{31})R(\frac{14}{31})R(\frac{28}{31})$ . It's image under rotation,  $RRRLL$ , visits the points obtained through the symmetry operation  $L(x) \rightarrow R(x)$  and  $R(x) \rightarrow L(x)$ . Coordinates visited by other orbits to period six are listed in Table I.

To compute the self RRR of the orbit  $LLLRR$  with itself, the crossing matrix for the five segments of this orbit is computed. It is

TABLE II: Crossing information for the four branches of the suspension of genus-3 dynamics shown in Fig. 5.

	<i>LL</i>	<i>LR</i>	<i>RL</i>	<i>RR</i>
<i>LL</i>	2	1	<i>a</i>	0
<i>LR</i>	1	2	1	<i>b</i>
<i>RL</i>	<i>a</i>	1	2	1
<i>RR</i>	0	<i>b</i>	1	2

- a* 1 if  $RL(s=1) > LL(s=1)$ , 0 otherwise.  
*b* 1 if  $LR(s=1) > RR(s=1)$ , 0 otherwise.

$$X = \begin{bmatrix} 2 & 2 & 1 & 0 & 0 \\ 2 & 2 & 1 & 0 & 0 \\ 1 & 1 & 2 & 0 & 1 \\ 0 & 0 & 0 & 2 & 1 \\ 0 & 0 & 1 & 1 & 2 \end{bmatrix} \begin{matrix} LL \\ LL \\ LR \\ RR \\ RL \end{matrix} \quad (3)$$

The integer matrix elements count the number of crossings of the different segments of this orbit with each other, and themselves. For example, the first segment *LL* (*LLLLRR*) crosses the third segment *LR* (*LLLLRR*) once. Counting crossings is relatively simple. The rules are summarized in Table II.

The next step is to represent the forward iteration operator by a permutation matrix. This describes how forward time evolution permutes the segments among each other. In the present case this is just a simple  $5 \times 5$  cyclic permutation matrix:

$$P = \begin{bmatrix} 0 & 1 & 0 & 0 & 0 \\ 0 & 0 & 1 & 0 & 0 \\ 0 & 0 & 0 & 1 & 0 \\ 0 & 0 & 0 & 0 & 1 \\ 1 & 0 & 0 & 0 & 0 \end{bmatrix} \quad (4)$$

The set of  $RRR_{ij}$  is expressed in matrix format as follows:

$$2N \times [RRR] = \sum_{k=1}^{k=N} P^k X P^{-k} \quad (5)$$

The sum over  $k$  extends to the smallest value of  $N$  for which  $P^N = Id$ . The factor 2 is present because the crossing matrix 4 counts crossings but the RRR is the average number of links (link =  $\frac{1}{2} \sum$  crossings). For the orbit *LLLLRR*,  $N = 5$  and

$$[RRR] = \frac{1}{2 \times 5} \begin{bmatrix} 10 & 4 & 2 & 2 & 4 \\ 4 & 10 & 4 & 2 & 2 \\ 2 & 4 & 10 & 4 & 2 \\ 2 & 2 & 4 & 10 & 4 \\ 4 & 2 & 2 & 4 & 10 \end{bmatrix} \quad (6)$$

The self RRR for this orbit are  $1^5(\frac{2}{5})^{10}(\frac{1}{5})^{10}$ . The unequal values of the off-diagonal fractions indicate that this orbit carries nonzero topological entropy [2].

The relative rotation rates for pairs of orbits follows the same set of steps. All  $p_A + p_B$  segments of the two orbits are located. The  $(p_A + p_B) \times (p_A + p_B)$  crossing matrix is constructed. The  $(p_A + p_B) \times (p_A + p_B)$  permutation matrix is the direct sum of the appropriate cyclic  $p_A \times p_A$  and  $p_B \times p_B$  matrices for each of the two orbits. The sum in Eq. (5) extend to  $N = p_A \times p_B$ , and the  $p_A \times p_B$  relative rotation rates  $RRR_{ij}(A, B)$  are contained in either of the  $p_A \times p_B$  off diagonal block submatrices.

## V. HOW TO COMPUTE $H_T$

A single orbit of period  $p$ , or a set of orbits of periods  $p_1, p_2, \dots$ , with  $p = p_1 + p_2 + \dots$ , intersects each Poincaré section in the genus-one suspension in exactly  $p$  points. The coordinates  $(x(s), y(s))_i$  vary as the parameter  $s$  increases from  $s = 0$  to  $s = 1$ . In a recently developed intuitive approach for computing topological entropy, the intersection points are used as vertices of simplices in the plane  $D^2$  [15]. As  $s$  increases degeneracies may occur: at these degeneracies the three vertices of a simplex become colinear. Algebraic rules relating the edges of the simplices before and after the singularity are used to evolve to an invariant description of the stretching and squeezing process in terms a subset of edges in the plane. A transition matrix that describes how the edges are stretched during a first return map is used to compute the topological entropy in the usual way. This measure is the logarithm of the largest eigenvalue of the transition matrix.

The particular suspension that we have introduced in Fig. 4 allows for spurious degeneracies, as all intersections are colinear at  $s = 0 \pmod{1}$ . To remove this problem it is useful to make a smooth diffeomorphism on the embedding, independent of position  $s$  along the flow. This generates a radius-dependent rotation of the form

$$\begin{pmatrix} x \\ y \end{pmatrix}' = \begin{bmatrix} \cos \theta & \sin \theta \\ -\sin \theta & \cos \theta \end{bmatrix} \begin{pmatrix} x \\ y \end{pmatrix} \quad \theta = \frac{\pi \sqrt{x^2 + y^2}}{(a + b + 1)} \quad (7)$$

This removes the problem of inessential singularities without altering the topology of the attractor, the topological organization of its unstable periodic orbits, or the computation of the topological entropy.

## VI. PREPARATION OF LORENZ DATA

Data generated by Lorenz dynamics have been embedded in a number of ways. In this section we introduce a new embedding method (braid embedding) for Lorenz data. The time series  $x(t)$  is recorded and the two components of the global Poincaré surface are defined as

	$x$	$\dot{x}$	$\ddot{x}$	
$L$	$> 0$	$= 0$	$< 0$	
$R$	$< 0$	$= 0$	$> 0$	

(8)

The transitions  $L \rightarrow L$  are directly read from the time series as successive maxima with  $x > 0$  and the transitions  $L \rightarrow R$  are directly read as transitions from a maximum with  $x > 0$  to a minimum with  $x < 0$ . The other two possible transitions  $R \rightarrow L$  and  $R \rightarrow R$  are similarly determined. This allows simple transformation of the time series to a symbol sequence.

Orbits of low period are extracted from the chaotic time series by appropriate methods (e.g., close returns). The “dynamical time”  $t$  (the time variable in the Lorenz equations) is converted into a “topological time”  $s$  in a systematic way. The topological time increases from  $s = 0$  to  $s = 1$  as the trajectory passes from one component of the Poincaré section to the next in its itinerary. One simple way to do this is to determine the (dynamical) times  $t_0, t_1, t_2, \dots, t_p$  that an orbit of period  $p$  intersects the components of a Poincaré section. A renormalization is given by

$$f(s) = \sum_{i=0}^p a_i(s) t_i \quad a_i(s) = \prod_{j \neq i} \frac{(s-j)}{(i-j)} \quad (9)$$

so that  $f(i) = t_i$ . This provides a simple lookup between the dynamical representation of the period- $p$  trajectory  $x(t)$  with  $t_0 \leq t \leq t_p$  and the topological representation  $x(s)$  with  $0 \leq s \leq p$ .

Since the interval between successive intersections is almost constant in Lorenz dynamics we used a simple interpolation for this renormalization from dynamical to topological time. With this parameterization we are able to look at the  $p$  intersections of a period- $p$  orbit with planes  $s = \text{const.}$ , and study how these intersections move about as  $s$  increases from 0 to 1.

In particular, we can use this representation to directly compute the set of relative rotation rates for pairs of orbits or the topological entropy of either single orbits or sets of orbits. We have done both sets of calculations on surrogate orbits extracted from chaotic time series generated by the Lorenz system for control parameters  $(R, \sigma, b) = (28.0, 10.0, 8/3)$ . The results are identical to those summarized in Tables III and IV.

## VII. DISCUSSION

It is possible to construct braid-like representations of branched manifolds that exist in genus- $g$  bounding tori when  $g > 1$ . These cannot be obtained by continuous deformation from the original branched manifold. Rather, the original must be cut and then glued back together. This cutting-gluing process is used to create branched

manifolds that are suspensions in genus-one tori of return maps that exist for flows in genus- $g$  bounding tori. This allows use of methods that have been developed for flows that are generated by stretching and folding mechanisms, and which exist within genus-one bounding tori.

In particular, we have computed relative rotation rates for flows in  $R^3$ . This is far from trivial, as RRR are only defined in toroidal phase spaces  $D^2 \times S^1$ , not in  $R^3$ . This is accomplished by mapping a flow from  $R^3$  to a suspension within a torus. The mapping procedure was described in Sect. III.

Once a braid representation is available, it is possible to construct two types of topological invariants: these are the set of rational fractions  $RRR_{i,j}(A, B)$  and the real numbers  $h_T(A)$ . These computations were carried out for orbits to period 6 in the Lorenz flow. The results are summarized in Table III. Computation of the RRR is simply done by projecting the orbit segments into the  $x$ - $s$  plane and counting crossings. We should point out here that orbits whose spectrum of self-relative rotation rates contain a single fractional value are well ordered ( $L, LR, LLR, LLRR, LLLRLR$ ) and those with two or more values are not well-ordered and therefore have positive topological entropy. Linking numbers of orbit pairs were computed by summing their mutual RRR. The results are presented in Table IV. The maximum number of different fractional values that such RRR can assume is equal to the greatest common divisor of the periods of the two orbits. Orbits with relatively prime periods have a single value for all their RRR. Linking numbers for orbit pairs exhibiting more than one fractional value for their mutual RRR, and which therefore imply a positive topological entropy (chaos) for the dynamical system, are shown in boldface.

Computation of the topological entropy is done by looking at intersections of the orbits with the  $(x, y)$  plane and looking for singularities in the simplices that cover the region of  $D^2$  that the orbits explore.

Although we have shown how to construct braid representations for branched manifolds in a genus-three bounding torus explicitly, these methods are applicable without change to branched manifolds that are contained in bounding tori with  $g > 3$ . The number of inequivalent bounding tori of genus  $g$  grows exponentially with a “genus” entropy of  $\log 3$  [12, 25]. Once this transformation has been carried out, it is possible to use methods developed for constructing topological invariants in simple tori  $D^2 \times S^1$  in cases where the three-dimensional dynamics is arbitrarily complicated (any  $g$ ).

Acknowledgements: RG thanks the CNRS for a visiting position at CORIA.

## REFERENCES

- [1] D. ECKMANN AND D. RUELLE, Ergodic theory of chaos and strange attractors, *Rev. Mod. Phys.* **57**,

TABLE III: Spectrum of self-RRR and the topological entropy  $h_T$  for orbits of period  $\leq 6$  in a genus-one suspension of a Lorenz flow. Orbits with a spectrum containing more than one distinct fractional value cannot be well-ordered and therefore carry a positive topological entropy.

Orbit	Spectrum of RRR	$h_T$
$\overline{L}$	$(1)^1$	
$LR$	$(1)^2(\frac{1}{2})^2$	
$LLR$	$(1)^3(\frac{1}{3})^6$	
$LLL$	$(1)^4(\frac{1}{2})^8(\frac{1}{4})^4$	
$LLRR$	$(1)^4(\frac{1}{4})^{12}$	
$LLLLR$	$(1)^5(\frac{1}{3})^{10}(\frac{2}{5})^{10}$	
$LLRRR$	$(1)^5(\frac{1}{5})^{10}(\frac{1}{5})^{10}$	
$LLRLR$	$(1)^5(\frac{1}{3})^{10}(\frac{2}{5})^{10}$	
$LLLLLR$	$(1)^6(\frac{1}{3})^{12}(\frac{1}{3})^{18}$	
$LLLLRR$	$(1)^6(\frac{1}{2})^{12}(\frac{1}{3})^{12}(\frac{1}{6})^6$	
$LLRLRR$	$(1)^6(\frac{1}{2})^{30}$	
$LLRRRR$	$(1)^6(\frac{1}{2})^{12}(\frac{1}{6})^{18}$	
$LLRLRR$	$(1)^6(\frac{1}{2})^{18}(\frac{1}{3})^{12}$	

TABLE IV: Linking numbers for orbits to period five. Bold-face entries indicate that the relative rotation rates for the two orbits are not all equal.

	1	2	3	4	5	6	7	8
$\overline{L}$	–	1	2	3	2	4	3	3
$LR$	1	–	4	<b>5</b>	4	6	5	7
$LLR$	2	4	–	7	6	9	7	9
$LLL$	3	<b>5</b>	7	–	<b>8</b>	12	10	12
$LLRR$	2	4	6	<b>8</b>	–	10	9	10
$LLLLR$	4	6	9	12	10	–	<b>13</b>	<b>15</b>
$LLRRR$	3	5	7	10	9	<b>13</b>	–	<b>12</b>
$LLRLR$	3	7	9	12	10	<b>15</b>	<b>12</b>	–

- 617 (1985).
- [2] H. G. SOLARI AND R. GILMORE, Relative rotation rates for driven dynamical systems, *Phys. Rev. A* **37**, 3096 (1988).
- [3] N. B. TUFILLARO, H. G. SOLARI, AND R. GILMORE, Classification of strange attractors by integers, *Phys. Rev. A* **41** 5717 (1990).
- [4] G. B. MINDLIN, H. G. SOLARI, M. A. NATIELLO, R. GILMORE AND X.-J. HOU, Topological analysis of chaotic time series data from the Belousov-Zhabotinskii reaction, *J. Nonlinear Science* **1**, 147 (1991).
- [5] R. GILMORE, Topological analysis of chaotic dynamical systems, *Rev. Mod. Phys.* **70**, 1455 (1998).
- [6] R. GILMORE AND M. LEFRANC, *The Topology of Chaos*, NY: Wiley, 2002.
- [7] D. ROLFSEN, *Knots and Links*, Berkeley, CA: Publish or Perish Press, 1976.
- [8] T. D. TSANKOV & R. GILMORE, Strange attractors are classified by bounding tori, *Physical Review Letters*, **91** (13), 134104, 2003.
- [9] T. D. TSANKOV & R. GILMORE, Topological aspects of the structure of chaotic attractors in  $\mathbb{R}^3$ , *Physical Review E* **69**, 056206 (2004).
- [10] E. N. LORENZ. Deterministic nonperiodic flow. *J. of the Atmos. Sci.*, **20**, 130-141, 1963.
- [11] T. SHIMIZU & N. MORIOKA. On the bifurcation of a symmetric limit cycle to an asymmetric one in a simple model, *Physics Letters A*, **76**, 201-204, 1980.
- [12] R. GILMORE AND C. LETELLIER, *The Symmetry of Chaos*, NY: Oxford University Press, 2007.
- [13] G. BYRNE, R. GILMORE & C. LETELLIER, Distinguishing between folding and tearing mechanisms in strange attractors, *Phys. Rev. E* **70**, 056214 (2004).
- [14] C. LETELLIER, T. D. TSANKOV, G. BYRNE, AND R. GILMORE, Large scale structural reorganization of strange attractors, *Phys. Rev. E* **72**, 026212 (2005).
- [15] M. LEFRANC, new paper on computing topological entropy
- [16] N. ROMANAZZI, M. LEFRANC, AND R. GILMORE Embeddings of low-dimensional attractors: Topological invariants and degrees of freedom, *Phys. Rev. E* **75**, 066214 (2007).
- [17] J. W. ALEXANDER, Topological invariants of knots and links, *Trans. Am. Math. Soc.* **30**, 275 (1923).
- [18] E. ARTIN, Theory of Braids, *Ann. Math.* **48**, 101 (1947).
- [19] J. BIRMAN, private communication.
- [20] J. BIRMAN AND R. F. WILLIAMS, Knotted periodic orbits in dynamical systems I: Lorenz's equations, *Topology*, **22**, 47-82, 1983.
- [21] J. BIRMAN AND R. F. WILLIAMS, Knotted periodic orbits in dynamical systems II: Knot holders for fibered knots, *Contemporary Mathematics*, **20**, 1-60, 1983.
- [22] C. LETELLIER & R. GILMORE, Covering dynamical systems : Two-fold covers, *Physical Review E*, **63**,

- 16206, 2001.
- [23] R. GILMORE, C. LETELLIER, AND N. ROMANAZZI  
Global topology from an embedding, *J. Phys. A*  
(submitted). oai:arXiv.org:0705.3427
- [24] R. GILMORE Two parameter families of strange at-  
tractors, *Chaos* **17**, 013014 (2007).
- [25] J. KATRIEL AND R. GILMORE, Entropy of bounding  
tori, (unpublished).
- [26] M. BESTVINA AND M. HANDEL, Train-tracks for  
surface homeomorphisms, *Topology* **34**, 109 (1995).
- [27] P. BRINKMANN, An implementation of the  
Bestvina-Handel algorithm for surface homeomor-  
phisms, *Experiment. Math.* **9**, 235 (2000).
- [28] T. HALL, Trainb: A C++ program for com-  
puting train tracks of surface homeomorphisms,  
[http://www.liv.ac.uk:maths/PURE/MIN.SET/CON  
TENT/members/THall.html](http://www.liv.ac.uk:maths/PURE/MIN.SET/CONTENT/members/THall.html).